OPEN ACCESS International Journal of Pharmacology

ISSN 1811-7775
DOI: 10.3923/ijp.2021.144.155

Research Article
Molecular Dynamics Study of MJ-33 and Derivatives Designed as cKit Kinase Inhibitors

[1,2]Hai-Anh Ha, [1]Mann-Jen Hour and [3]Jai-Sing Yang

[1]School of Pharmacy, China Medical University, Taichung 40402, Taiwan, Republic of China
[2]Faculty of Pharmacy, Duy Tan University, Da Nang 550000, Vietnam
[3]Department of Medical Research, China Medical University Hospital, China Medical University, Taichung 40447, Taiwan, Republic of China

Abstract

Background and Objective: Due to the high mortality rate, cancer is still a burden to society and therefore, the development of anticancer therapies is necessary. In our lab, a quinazolinone compound (MJ-33) was synthesized and showed an inhibitory effect on several types of cancer cells. However, the direct biological target was not clarified. This study aimed to investigate possible molecular targets of MJ-33. **Materials and Methods:** In a computational approach, 2-step *in silico* screening, using molecular docking and Molecular Dynamics (MD) simulation was carried out to identify top-high affinity and most stable targets of MJ-33. MD simulations in 100 ns were performed to identify intermolecular interactions and structural insights of ligand-protein complexes. **Results:** MJ-33 has a strong affinity with cKit kinase. During the simulation course, the MJ33-cKit complex remained stable and no large conformational change of the protein was detected. Besides, an MJ-33 derivative (C93) was proposed as a potential cKit inhibitor. C93 may establish a complex with cKit kinase with several improvements for complex stability and intermolecular interactions, compared with those of MJ-33. **Conclusion:** In summary, our study suggested that cKit kinase is possibly the direct biological target of MJ-33. Based on the structural insight of the MJ33-cKit complex and MJ-33 scaffold, a rational drug design was carried out to propose a promising cKit inhibitor to be developed in the future.

Key words: MJ-33, cKit inhibitor, receptor tyrosine kinase, anticancer, molecular dynamics, MJ-33 derivatives, binding pocket

Citation: Ha, H.A., M.J. Hour and J.S. Yang , 2021. Molecular dynamics study of MJ-33 and derivatives designed as cKit kinase inhibitors. Int. J. Pharmacol., 17: 144-155.

Corresponding Authors: Mann-Jen Hour, School of Pharmacy, China Medical University, 91 Hsueh-Shih Road, Taichung 40402, Taiwan, Republic of China Jai-Sing Yang, Department of Medical Research, China Medical University Hospital, China Medical University, 2 Yude Road, Taichung 40447, Taiwan, Republic of China

Competing Interest: The authors have declared that no competing interest exists.

Data Availability: All relevant data are within the paper and its supporting information files.

INTRODUCTION

Cancer mortality rates remain high despite advances in early detection and improvements in therapeutic development. As such, cancer remains a burden on patients, the healthcare system and society[1], therefore, the discovery of new anticancer drugs is important. Receptor Tyrosine Kinases (RTKs) play an important role in cancer biology and targeting them may provide a strategy for developing novel cancer therapeutics[2,3]. Several Tyrosine Kinase Inhibitors (TKIs) have been approved for therapeutic use in a certain type of cancers, such as lung cancer, lymphoma or colorectal cancer[4-6]. Therefore, the development of new TKIs may provide a route to improve treatment effectiveness, facilitate personalized treatment and also alleviate concerns surrounding drug resistance.

The quinazolinone compound, MJ-33 (2-(3-ethoxyphenyl) -6-(pyrrolidin-1-yl) quinazolin-4(3H)-one), was synthesized in our laboratory and has previously been studied for its anticancer effect; it is associated with the inhibition of MAPK, AKT, NF-kappaB and AP-1 signal-transduction pathways[7,8]. These studies suggested that the MJ-33-induced anticancer effect may be initiated by an upstream-signal regulator of these pathways. Additionally, our previous evidence revealed that an MJ-33-analog (MJ-56) induced anticancer activities through inhibition of RTKs[9]. Taken together, this data suggests that RTKs are the biological target that confer the anticancer effects of MJ-33.

The activation of RTKs signalling cascade (e.g., by the gene cKit) is normally triggered by its ligand (stem cell factor) upon binding to the extracellular domain of the receptor[10]. This biological event results in dimerization with a nearby RTK, which consequently triggers the signal transduction cascade (with the participation of ATP and Mg^{2+}) on the intracellular kinase domain[10,11]. A type-I TKI (e.g, Sunitinib) acts as a ligand to form a complex with an intracellular kinase domain in an inactivated conformation, which subsequently leads to inhibition of kinase enzymatic activity by occupying the ATP-binding pocket[11,12].

Since the molecular mechanism of TKIs is initiated by a direct interaction of ligand and protein[2,13,14], ligand-protein interaction studies have great potential for investigating drug targets and can also be utilized in rational drug design[15]. Recent advances in computational tools have helped facilitate drug discovery, through molecular modelling, pharmacophore mapping and Molecular Dynamics (MD) simulation[16].

In this study, we used an *in silico* approach to investigate the possible target of MJ-33. We also analyze the molecular interactions of MJ-33 with its protein receptor and examine the stability of the ligand-protein complex through MD simulation. This data was subsequently used to carry out a structure-based drug design aimed at improving intermolecular interactions and consequently the stability of the ligand-protein complex.

MATERIALS AND METHODS

Study area: The study was carried out at the School of Pharmacy and the Department of Medical Research, China Medical University Hospital, China Medical University from March, 2020-February, 2021.

Ligand modelling and preparation: From SMILES code, 3-dimensional (3D) ligand models were built using the tool menu of UCSF Chimera (version 1.13.1-Regents of the University of California). All the ligand models were energy-minimized by the Obminimize module of Open Babel (version 3.0.1), using a Chemical force field of 2500 steps. Output files were then converted by the Open Babel into PDBQT format and saved for further use in the docking process.

Protein model preparation: Our study examined RTKs as target proteins; therefore, we obtained a list of RTKs from previous studies that conducted Inverse Virtual Screening (IVS) on potential anticancer targets[17-19]. The Protein Data Bank (PDB) ID of proteins was used to download corresponding molecular models from the Research Collaboratory for Structural Bioinformatics (RCSB) PDB (http://www.pdb.rcsb.org). Before the docking process, the Chimera UCSF software was used to check and remove all non-standard residues and solvents in the co-crystallized PDB models.

Molecular docking: The software package used to assess molecular docking was AutoDock Vina (version 4.26-The Scripps Research Institute)[20]. Chimera UCSF software was used to visually examine the protein and binding site. The grid box for docking was built for each PDB code according to The Computer Atlas of Surface Topography of Proteins (CASTp3.0), this information was also cross-referenced with previously published studies[17-19]. The exhaustiveness parameter of AutoDock Vina was set to 128 for every docking process. All molecular docking was conducted using a command-line interface. The PoseView software (version 1.1.2, BioSolveIT) and UCSF Chimera were used to check the binding patterns and molecular interactions between ligands and proteins.

Drug-likeness analysis: Swiss ADME (Swiss Institute of Bioinformatics) provided tools for analyzing basic characteristics of small molecules. SMILES codes of ligands were collected for input at the web-based service (http://www.swissadme.ch/) to assess drug-likeness and basic physicochemical property analysis.

Molecular dynamics simulation: To assist ligand-protein complex preparation, UCSF Chimera was used to identifying the best docking mode from the molecular docking result. Molecular dynamics simulations in 5 and 100 ns were set up for different purposes. The reference temperature was set to 300 K and pressure was set to 1 atm in all setup.

For preliminary screening purposes, we used GROMACS (version 2020.1-Ubuntu-2020.1-1) to run short MD simulations (5 ns) for each complex. The CHARMM36 General Force Field (CGenFF version 4.4, updated July, 2020) was used for topology generation of both protein and ligand. The TIP3P water model was used as a solvent in a defined box around the complex. Sodium and chloride ions were selected for charge neutralization in the simulation system. Energy minimization (50,000 steps, energy step size 0.01) was conducted before equilibration stages (both NVT and NPT, 50,000 steps for each). The equilibrated system was set to run MD production in the desired simulation time. The output trajectory was analyzed for ligand Root Mean Square Deviation (RMSD) fitting to the protein following 5 ns duration.

Further investigation of intermolecular interaction requires longer simulation and advanced analysis tools. Promising ligand-protein complexes were selected to perform MD simulations for 100 ns as previously described[21,22]. The module Desmond Molecular Dynamics System, (version 6.0, D. E. Shaw Research, Schrodinger® 2019-4) was used for this purpose and the system was generated using the OPLS_2005 force field. As before, the solvent system was built with TIP3P water around the complex. Sodium cations and chloride anions were used for system charge neutralization. After energy minimization, for both the NVT and NPT ensembles, the MD run was set to 100 ns of simulation. Output data was analyzed for RMSD, Root Means Square Fluctuation (RMSF), ligand-protein contacts and conformational evolution using built-in plugins of the software.

RESULTS

Molecular docking of MJ-33 on selected RTKs and preliminary screening by MD simulation: To explore the possibility of an interaction between MJ-33 and RTKs, we conducted molecular docking of MJ-33 as a ligand on ATP-binding pockets of RTK models. In total, 12 PDB IDs, corresponding to 12 RTKs were selected for this study. Results in Table 1 show that the MJ-33 molecule fits at the desired binding pockets and shows strong affinity with several RTKs. The top-scoring receptors, in terms of affinity, were tyrosine-protein kinase (ABL1), cKit-kinase, BTK and ABL2. As the docking algorithm of AutoDock Vina is based on the flexibility of the ligand within a rigid binding site, further investigation was required to predict the stability of the ligand within the binding pocket. For this purpose, we conducted a short-time simulation using the GROMACS software package to determine the ligand deviation in the complexes. The top four complexes were selected for 5 ns simulation and the RMSD of MJ-33 was analyzed. The data of Fig. 1 shows that MJ-33, when in a complex with cKit is the most stable compared to other complexes during the simulation time, with a ligand-RMSD value maintained under 3 Angstroms. This preliminary data suggests that MJ-33 may have stable intermolecular interactions with ATP-binding pocket residues of cKit kinase. According to molecular docking results (Fig. 2a-b), MJ-33 has several interactions with adjacent residues, such as formable

Table 1: Docking scores of MJ-33 on receptor tyrosine kinases

Receptor name	PDB ID	Docking score (kcal mol^{-1})
Tyrosine-protein kinase ABL1	2HYY	-10.5
Mast/stem cell growth factor receptor (cKIT-kinase)	3G0E	-10.4
Tyrosine-protein kinase ABL2	3HMI	-9.7
Tyrosine-protein kinase BTK	5P9I	-9.6
RET tyrosine kinase	2X2K	-9.5
Vascular endothelial growth factor receptor 2 (VEGFR2)	3EWH	-9.5
Tyrosine-protein kinase Src	3F3V	-9.4
Receptor tyrosine-protein kinase erbB-4	3BBT	-9.3
Insulin-like growth factor I receptor	2OJ9	-9.0
Hepatocyte growth factor receptor (c-Met kinase)	2WD1	-8.3
Epidermal growth factor receptor (EGFR)	2J5F	-7.7
Heparin-binding growth factor 1	1HKN	-6.6
Vascular endothelial growth factor receptor 1 (VEGFR1)	1FLT	-6.1

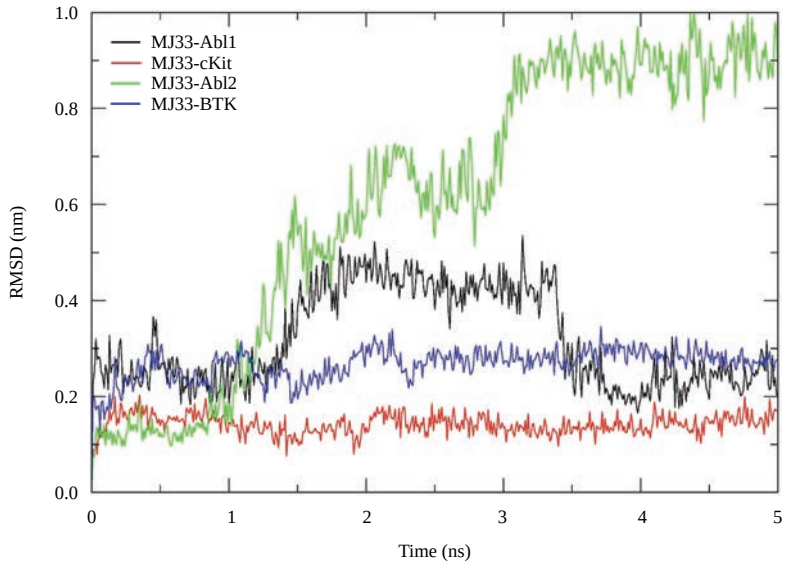

Fig. 1: RMSD least-squares fitting to the protein of MJ-33 in complex with selected receptor tyrosine kinases

Black: MJ-33 in complex with tyrosine-protein kinase ABL1. Red: MJ-33 in complex with cKit kinase. Green: MJ-33 in complex with tyrosine-protein kinase ABL2. Blue: MJ-33 in complex with Bruton's Tyrosine Kinase (BTK)

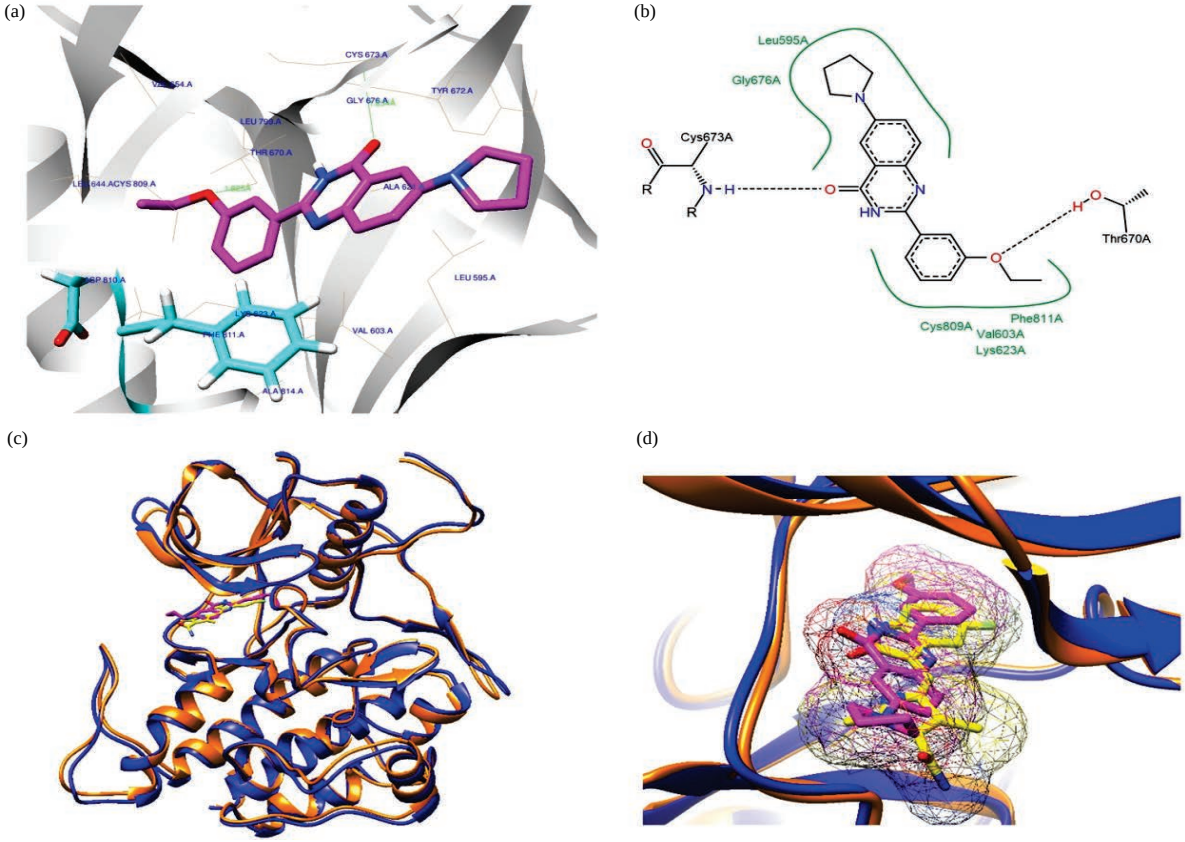

Fig. 2(a-d): Binding pattern of MJ-33 in the ATP-binding site of cKit kinase

(a) Docking pose of MJ-33 in ATP-binding pocket with adjacent residues, (b) 2-dimensional plot of MJ-33 docking mode on cKit kinase, (c) Overall structural matching of cKit kinase after 5ns-simulation (blue) versus co-crystallized conformation (orange) and (d) Superposition view of MJ-33 (magenta) and Sunitinib (yellow) in the ATP-binding pocket of cKit kinase

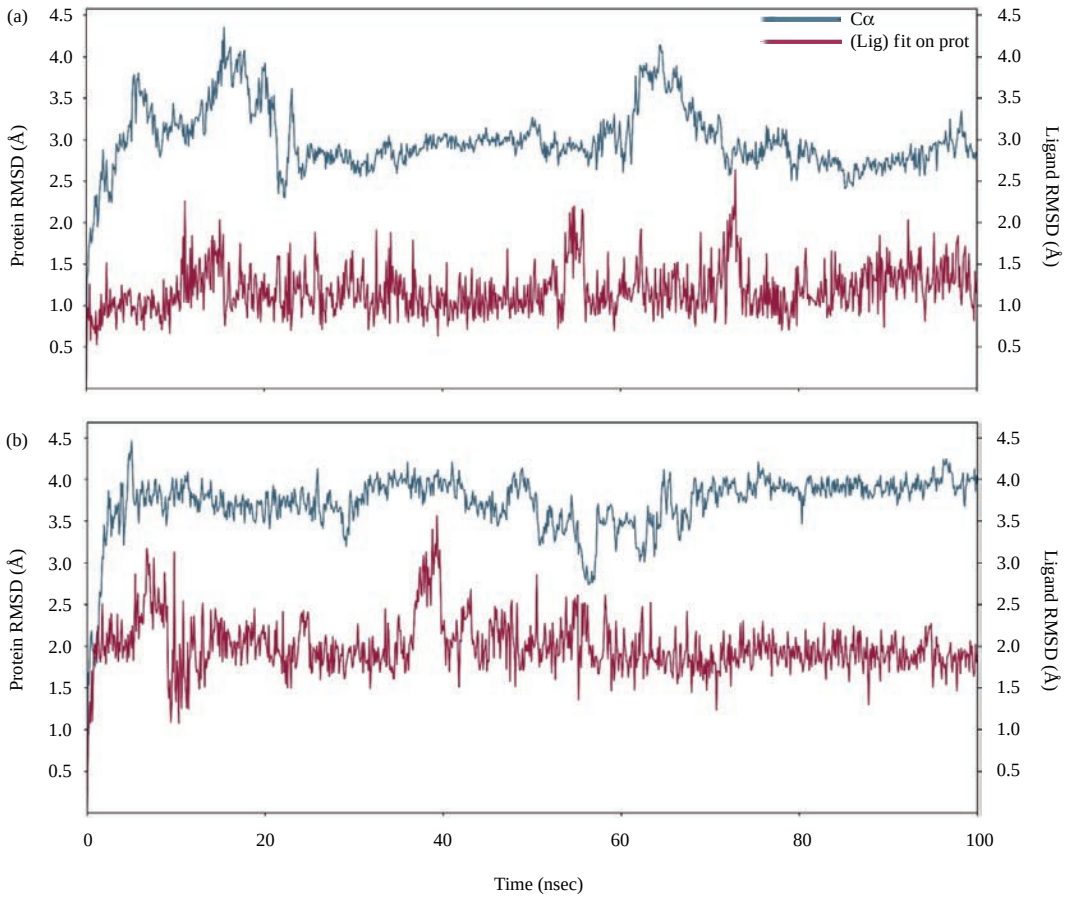

Fig. 3(a-b): 100 ns-RMSDs of ligand versus protein of MJ33 and Sunitinib in complex with cKit kinase
(a) MJ33-cKit and (b) Sunitinib-cKit

H-bonds with Cys673 and Thr670 and other hydrophobic interactions with Leu595, Val603, Lys623, Gly676, Cys809 and Phe811. Based on docking scores and initial simulation data, we selected the MJ33-cKit complex for further investigation, to explore the structure and ligand-protein interactions.

Binding pattern analysis and conformational changes of MJ33-cKit complex after short-time simulation: Using visualization software (USCF Chimera), we examined the 3-D view of the MJ33-cKit complex, which was identified from the docking result. The data of Fig. 2a shows a PoseView of MJ-33 (magenta) in the ATP-binding pocket of cKit, next to the DFG residues (Asp810-Phe811-Gly812) which are presented in cyan and red. The intermolecular interactions of MJ-33 with cKit are presented as a simplified 2-dimensional (2D) diagram in Fig. 2b. Results show evidence of 2 H-bonds, with Cys673 and Thr670, on this binding pattern. Other hydrophobic interactions with Leu595, Gly676, Cys809, Val603, Lys623 and Phe811 were also involved in the binding mode of MJ-33.

To observe the overall change in protein conformation, we extracted the last frame from the 5 ns simulation course. Using the MatchMaker tool of USCF Chimera, the protein conformation was aligned with the co-crystallized model (PDB ID 3G0E). As shown in Fig. 2c, following 5 ns simulation, the cKit model (blue) displayed no large conformational differences when compared to the crystallized model (orange). A superimposed view of the MJ-33 molecule (magenta) with native inhibitor (Sunitinib, yellow) is shown in Fig. 2d. The spatial overlapping of 2 small molecules (MJ-33 and Sunitinib) in the same ATP-binding pocket suggests that MJ-33 may act as an ATP-competitor to inhibit cKit kinase, similar to that mechanism of Sunitinib.

Structural insight of MJ33-cKit complex during 100 ns of simulation, in comparison with Sunitinib: Since we hypothesized that MJ-33 is a potential cKit inhibitor, a long-timescale simulation was carried out to elucidate the stability of the ligand-protein complex. We conducted a 100 ns simulation study on the MJ33-cKit complex. Ligand-RMSD and protein-RMSD of the MJ33-cKit complex were monitored during the simulation time, as shown in Fig. 3a. Data indicated that the protein-RMSD was less than 4.5 Angstroms and

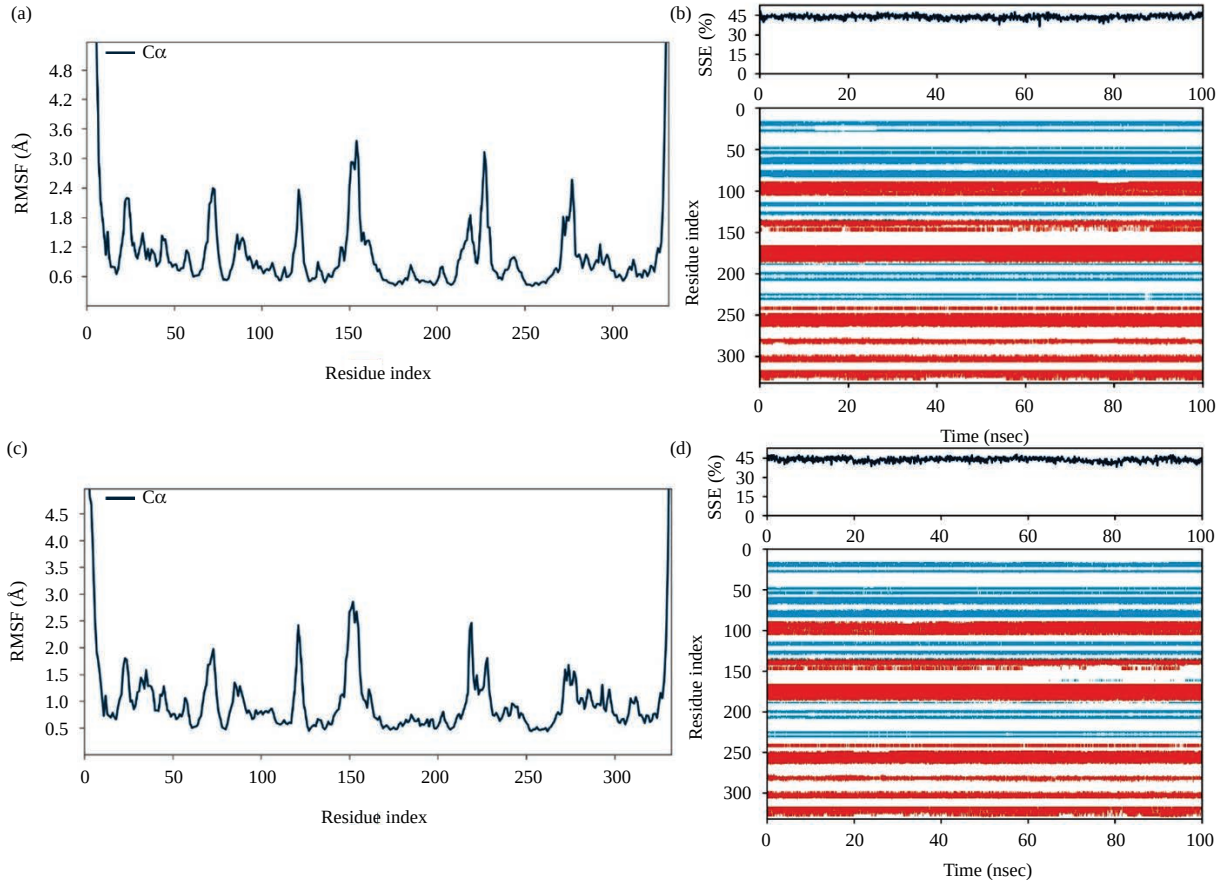

Fig. 4(a-d): RMSFs and secondary structure elements of cKit after complexed with MJ-33 and Sunitinib

(a) RMSF and (b) Secondary structure elements of cKit in complex with MJ-33, (c) RMSF and (d) Secondary structure elements of cKit in complex with Sunitinib

mostly ranged from 2.5-3.5 Angstroms. However, the ligand-RMSD received a lower value than protein-RMSD, in the range of 0.5-1.5 Angstroms. This result supports our hypothesis of the stability of our model MJ33-cKit complex in a simulation system. For a reference model, we used a co-crystallized complex of cKit (PDB ID 3G0E) with a native inhibitor (Sunitinib) to conduct an MD simulation under the same parameters. The results presented in Fig. 3b demonstrate that this protein-RMSD was also less than 4.5 Angstroms, whilst the ligand-RMSD was mainly distributed in the range of 1.0-2.0 Angstroms. Overall, we were able to observe that the deviation pattern of both MJ33-cKit and Sunitinib-cKit complexes were within an acceptable range and can be considered stable in the simulation system (Fig. 3a-b). The low protein-RMSDs values also suggested that there were no large conformational changes in the protein secondary structure of both complexes. Ligand-RSMD values lower than protein-RSMDs suggest the ligands were stable in the binding pockets in both complexes.

To gain a better understanding of the structural insight of the protein model in a simulation, we analyzed trajectory output data for RMSF and secondary structure changes. In the MJ33-cKit complex, except for 2 terminal-residues, which displayed fluctuating ranges, all the other fluctuations were lower than 3.6 Angstroms (Fig. 4a). The Secondary Structure Element (SSE) composition histogram was shown in Fig. 4b indicated that the protein fluctuations did not trigger a large conformational change of cKit. Despite several temporary swapping of secondary structures were detected, SSE assignment for each residue during the simulation course, but these changes did not affect overall SSE, indicating overall stability of protein structure of cKit. Similarly, the RMSF histogram of cKit in complex with Sunitinib (Fig. 4c) indicated no unexpected fluctuation observed. The SSE composition histogram of the Sunitinib-cKit complex (Fig. 4d) indicated no large conformational change of the protein as well.

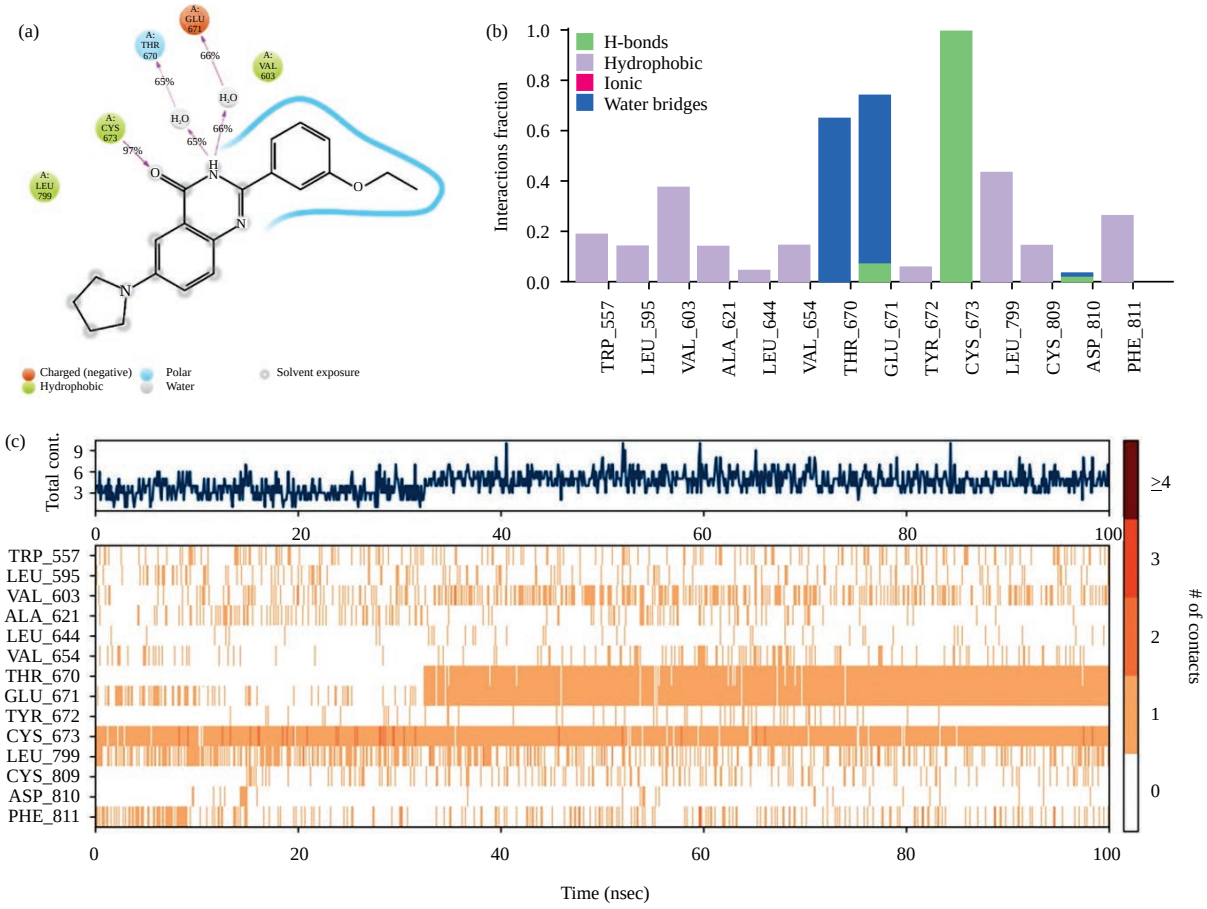

Fig. 5(a-c): Contact analysis of MJ-33 with adjacent residues during the 100 ns-simulation course

(a) Ligand-protein contact analysis of MJ33-cKit complex in 2-dimensional plot, (b) By fractions of contact types and (c) In a histogram of 100 ns

Ligand-protein contact analysis of MJ33-cKit complex: The intermolecular contacts between MJ-33 and cKit in the simulation complex were analyzed. Our result revealed that the MJ-33 molecule maintained an H-bond with Cys673 for 97% of the simulation duration (Fig. 5a-b). This supports our hypothesis that the position of MJ-33, relative to the protein, remained stable in the simulation system. In the timeline presentation of ligand-protein contacts (Fig. 5c), there was an increased number of contacts of MJ-33 with residues Thr670 and Glu671 following 32 ns simulation. When examining analyzed data of ligand-protein contact and fractions of contact types, we can identify that the contacts of MJ-33 with Thr670 and Glu671 were newly formed by water-bridge H-bonds. This observation revealed that the solvent penetrated from other locations into the binding cavity and joined the intermolecular interaction of the ligand and protein.

MJ-33 derivatives designed as potential cKit inhibitors: The ATP-binding pocket of cKit is narrow, therefore, the occupied volume of the ligand is important. As there is limited free space around the scaffold within the binding cavity (Fig. 6a), only a small substitution group is acceptable. Besides, as presented in Fig. 6a, the binding pocket can be divided into the hydrophilic area (blue-white colour), corresponding to the solvent-exposed tail of the ligand and hydrophobic area (orange-brown colour).

Our observations of the 3D model views showed the optimal positions for substitutions (Fig. 6b). The R_1-substitution may have increased the intermolecular contact of the ethoxy phenyl fragment to neighbouring residues at the hydrophobic area. In particular, R_1 can be substituted by an H-bond donor to match with an H-bond acceptor nearby (Thr670). Additionally, R_1-substitution may also increase hydrophobic contact between the aromatic ring of an ethoxy phenyl fragment to the Phe811 residue. To limit water-bridged contact in the binding cavity, the R_2-substitution group was designed adjacent to the hydrophilic area, to act as an impediment to prevent water from penetrating the binding pocket.

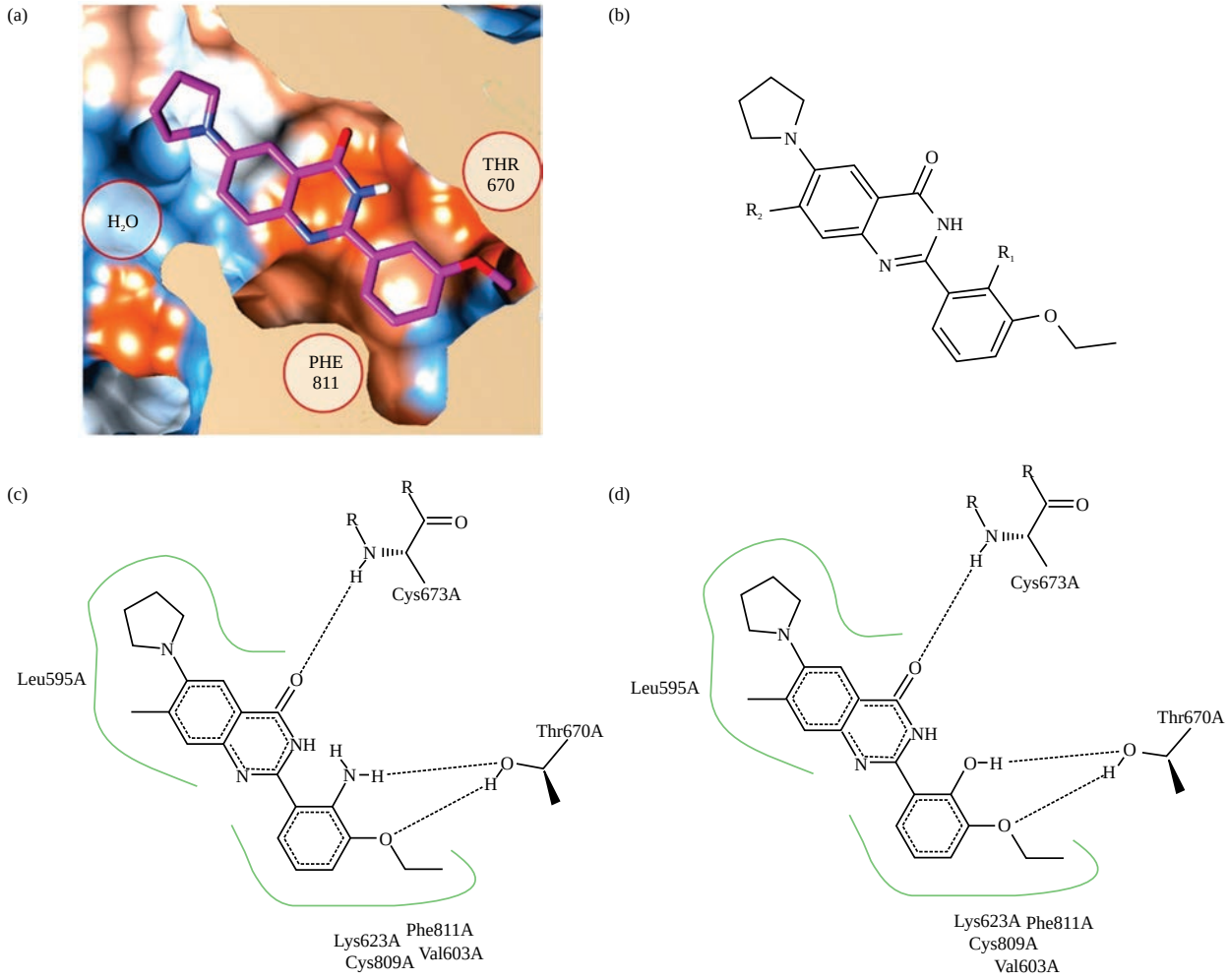

Fig. 6(a-d): Designing MJ-33 derivatives as potential cKit inhibitors

(a) Key adjacent residues, hydrophobic/hydrophilic view of MJ-33 in the binding site. (b) Substitutional positions (R_1 and R_2) on MJ-33 scaffold and (c-d) Binding pattern of newly designed structures on ATP-binding pocket of cKit kinase

From above analysis, we designed 2 new structures: C85 (with R_1 = -OH; R_2 = -CH_3) and C93 (with R_1 = -NH_2; R_2 = -CH_3). 3D models of these newly designed structures were constructed and molecular docking was performed (as previously described). Molecular docking results presented in Table 2 show better docking affinity of both C85 and C93, in comparison with that of the MJ-33 scaffold. Additionally, predicted physicochemical properties for newly designed structures implied that C85 and C93 confirmed with general rules of small-molecule drug design (Table 2). The binding pattern of C85 and C93 are depicted in Fig. 6c-d and show that both had more H-bond interaction, compared to the binding pattern of MJ-33. The newly designed structures showed a promising ligand at the ATP-binding pocket of cKit kinase. Thus, we selected the best docking-scored structure (C93) for further investigation.

Result of molecular dynamics study on C93-cKIT complex through 100 ns simulation: Using the same approach as for simulation study on complexes of MJ33-cKit and Sunitinib-cKit, we investigated the molecular dynamics properties of C93-cKit in a 100 ns simulation system. The ligand-RMSD and protein-RMSD of the C93-cKit complex are presented in Fig. 7a. The ligand-RMSD was mainly below the protein-RMSD, which implied that C93 was held steady inside its binding cavity during simulation time. The values of these 2 RMSDs were both lower than 3 Angstroms, considerably better than that of both MJ-33 and Sunitinib. This result supported our hypothesis that C93 may establish a more stable complex with cKit kinase than the original scaffold (MJ-33).

The data of Fig. 7b shows the RMSF histogram where there is no unexpected fluctuation observed throughout protein residues of cKit. Except for the natural

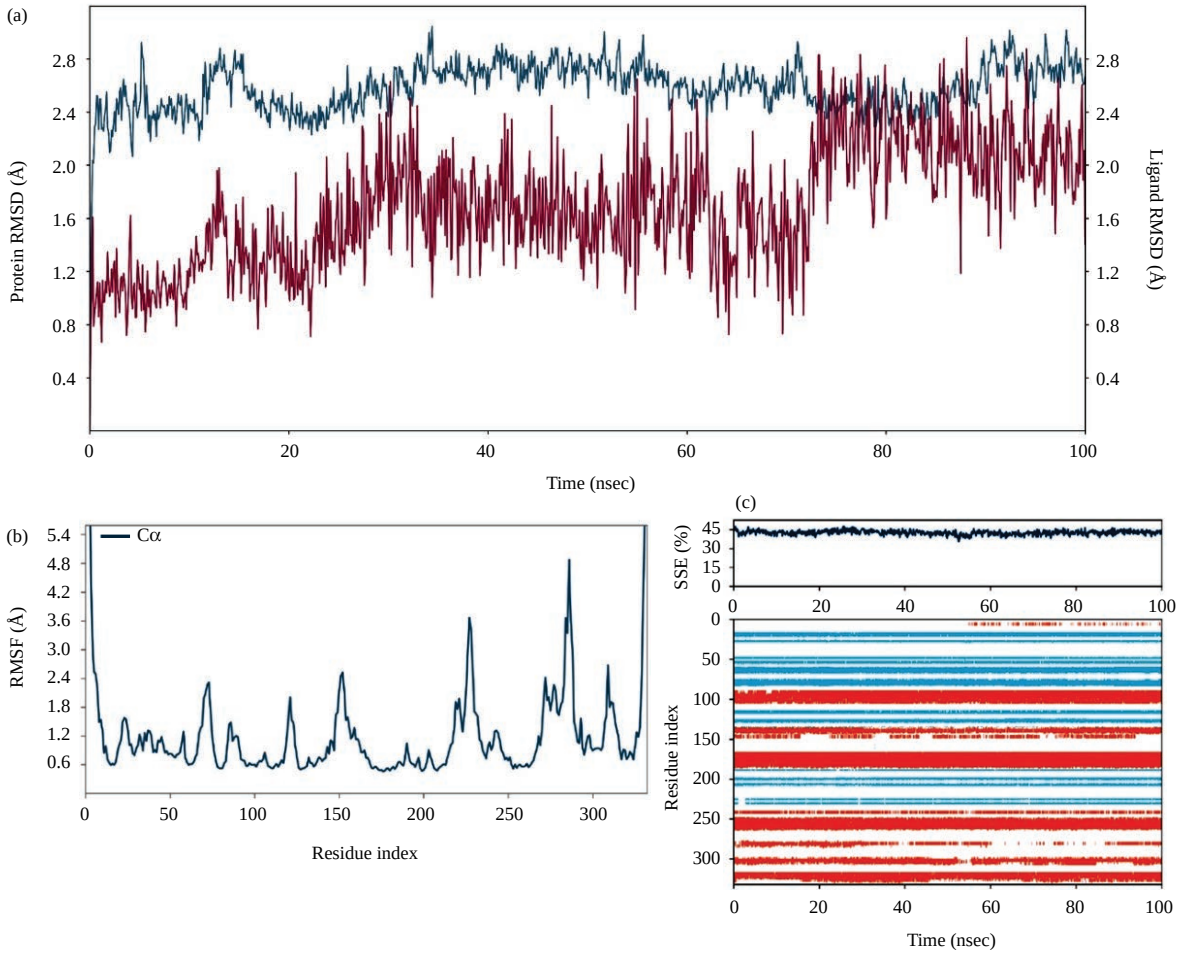

Fig. 7(a-c): Structural insights of C93-cKit complex in 100 ns simulation course

(a) RMSDs of ligand versus protein of C93-cKit complex, (b) RMSF of cKit kinase after complexed with C93 and (c) Secondary structure features of cKit kinase after complexed with C93

Table 2: Docking scores and predicted physicochemical properties of MJ-33 and designed structures

Compound	Docking score (kcal mol^{-1})	H-bond acceptor/donor	TPSA (Å^2)	Consensus Log P (o/w)	GI absorption	Lipinski violation
C93	-10.9	3/2	84.24	3.23	High	No
C85	-10.8	4/2	78.45	3.36	High	No
MJ-33	-10.4	3/1	58.22	3.40	High	No
Sunitinib	-9.6					

TPSA: Topological polar surface area, GI: Gastrointestinal

fluctuation of 2 terminals of the protein chain, most of the RMSF curve was below the acceptable value of 5 Angstroms. As summarized in the Secondary Structure Element (SSE) composition histogram (Fig. 7c), the protein fluctuations did not trigger a large conformational change of cKit. SSE assignment for each residue during the simulation course detected several temporary swapping of secondary structures, but this did not affect overall SSE and indicated overall stability of protein structure (Fig. 7c).

Ligand-protein contacts in C93-cKit complex: The interactions of C93 with cKit residues within the binding pocket were analyzed and depicted in a 2D form in Fig. 8a (only residues that interacted for more than 30% of simulation time are shown). The fraction of protein-ligand interactions is shown in Fig. 8b. The established H-bonds were detected between C93 and Cys673 and Thr670 with retention rates of 99 and 46%, respectively during simulation. Additionally, the hydrophobic contacts of C93 with Phe811, Leu799 and Leu595 were also identified. The timeline data (Fig. 8c)

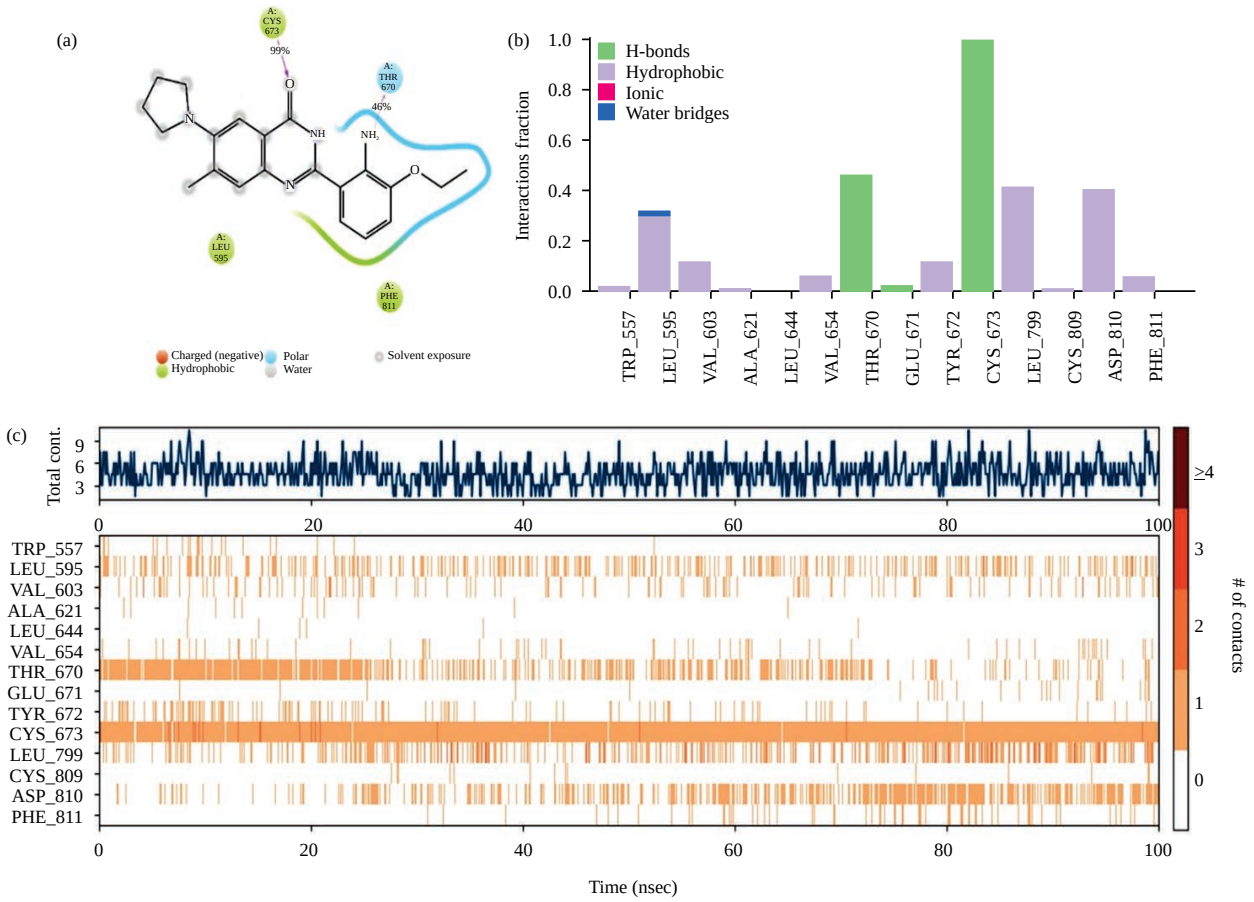

Fig. 8(a-c): Contact analysis of C93 with adjacent residues during the 100 ns-simulation course
(a) Ligand-protein contact analysis of C93-cKit complex in 2-dimensional plot, (b) By fractions of contact types and (c) In a histogram of 100 ns

provided us with more detail about the evolution of C93-cKit intermolecular contacts. Compared with the results of MJ-33 (Fig. 5a), C93 received a greater number of direct H-bond, eradicated all water-bridged H-bonds with Thr670 and Glu671 and gained more direct interaction with the Phe811 residue. Collectively, the C93-cKit intermolecular interactions in our simulation system indicated that the aims of designing new derivatives based on the MJ-33 scaffold were achieved and C93 is a representative result.

DISCUSSION

In this study, using molecular docking and MD simulation, our 2-step *in silico* screening revealed that, cKit kinase is the promising direct target of MJ-33. The combination strategy of molecular docking and MD simulations[23] was applied in this study for both target screening and drug designing. The selected target, cKit kinase did not receive the best docking score (Table 1), but the preliminary simulation (Fig. 2a) emphasized that it is the most promising stable binding target of MJ-33. Following that, the long-timescale simulation result for the MJ33-cKit complex (Fig. 3a) showed a good relative RMSD histogram of ligand versus protein, as well as when compared with that of Sunitinib-cKit complex (Fig. 3b). The co-crystallized model (PDB ID 3G0E) was identified as an inactivated conformation of cKit, which in complex with Sunitinib is an inhibitor at ATP-binding site[12]. To act as an inhibitor, the ligand should maintain the ligand-complex stability to prevent kinase transactivation[10] and minimize rejection from the ATP-binding site. In combination with the RMSF and SSE analysis results (Fig. 4a-b), this data supports the notion that MJ-33 may act as a ligand in complex with cKit kinase and this complex may share molecular dynamic characteristics similar to Sunitinib.

As reported previously, MJ-33 effectively inhibits multiple signalling pathways (MAPK, AKT, NF-kappaB and AP-1) in prostate DU145 cells[7] and blocks AKT signal in the 5FU-resistant colorectal HT29 cells[8]. Both DU145 and HT29 cell lines are cKit-positive[24,25] and are characterized by cKit overexpression. Although further experimental research is

needed, this study provides preliminary data supporting the hypothesis that the MJ-33-induced anticancer effects are possibly due to the interaction between MJ-33 and cKit kinase.

Understanding the intermolecular interaction behaviours of MJ-33 with cKit under a simulation system facilitates rational drug design. MJ-33 has a molecular weight of 335.4 (g mol^{-1}), 4 rotatable bonds, 3 H-bond acceptors and 1 H-bond donor. Thus, MJ-33 meets both requirements of a drug-like and lead-like compound[26]. In our drug design, we used MJ-33 as a scaffold for designing derivatives that could act as new potential ligands of cKit. In our simulations of cKit complexed with newly designed compound, molecular flexibility of ligand and protein, the impact of solvent and complex stability were monitored. We successfully demonstrated improvements in docking pattern, stability of the complex, as well as intermolecular interactions. The ligand design for C93 enhanced docking affinity (Table 2), decreased protein RMSD value (Fig. 8a) and eradicated unwanted water-bridged interactions (Fig. 7a), compared to those of the original scaffold. Besides, the interaction between C93 and Phe811 was increased. The orientation of Phe811 and protein-folding were associated with each other by the DFG-motif, an important factor that accounts for the conformation change and activation of tyrosine kinase[3]. The increasing direct interaction of ligand to Phe811 may contribute to the "DFG-flip" for conformational transition, which is required for tyrosine kinase activation[10,27].

The new structure of C93 is intentionally designed with minor structural changes, assuming that general biological activity may be inherited from the lead compound (MJ-33). The structural features of C93 are designated for cKit binding and as such, the specificity of C93 for cKit kinase may be expected. Further experimental studies on C93 should be carried out to identify chemical synthesis. Future studies should also investigate anticancer effects on certain types of cancer, in particular in cell lines over expressing cKit.

CONCLUSION

In conclusion, the present study provides the structural insight of cKit kinase as a potential target for novel quinazolinone MJ-33 for inducing its anticancer effect. Additionally, a derivative of MJ-33 (C93) was designed for targeting cKit kinase and shows a promising structure and should undergo further synthesis and development as a cKit inhibitor. The findings of this study were obtained by an *in silico* approach, therefore more experimental work is required for further confirmation in the biological model.

SIGNIFICANCE STATEMENT

This study discovers the cKit kinase as possible direct target of MJ-33 and derivatives that can be beneficial for further study on synthesizing new compounds, targeting cKit kinase for inducing anticancer effect, as well as investigating the underlying molecular mechanism. This study will help the researcher to uncover the critical areas of drug target identification and drug design in a particular target that many researchers were not able to explore. Thus, a new theory on *de novo* rational drug design may be arrived at.

REFERENCES

1. Siegel, R.L., K.D. Miller and A. Jemal, 2020. Cancer statistics, 2020. C.A. Cancer J. Clin., 70: 7-30.
2. Jiang, W. and M. Ji, 2019. Receptor tyrosine kinases in PI3K signaling: The therapeutic targets in cancer. Seminars Cancer Biol., 59: 3-22.
3. García-Aranda, M. and M. Redondo, 2019. Targeting receptor kinases in colorectal cancer. Cancers, Vol. 11. 10.3390/cancers11040433.
4. Al-Salama, Z.T. and S.J. Keam, 2019. Entrectinib: First global approval. Drugs, 79: 1477-1483.
5. Syed, Y.Y., 2020. Zanubrutinib: First approval. Drugs, 80: 91-97.
6. Shah, R. and J.F. Lester, 2020. Tyrosine kinase inhibitors for the treatment of EGFR mutation-positive non–small-cell lung cancer: A clash of the generations. Clin. Lung Cancer, 21: e216-e228.
7. Hour, M.J., S.C. Tsai, H.C. Wu, M.W. Lin and J.G. Chung *et al*., 2012. Antitumor effects of the novel quinazolinone MJ-33: Inhibition of metastasis through the MAPK, AKT, NF-kappaB and AP-1 signaling pathways in DU145 human prostate cancer cells. Int. J. Oncol., 41: 1513-1519.
8. Ha, H.A., J.H. Chiang, F.J. Tsai, D.T. Bau and Y.N. Juan *et al*., 2021. Novel quinazolinone MJ-33 induces AKT/mTOR-mediated autophagy-associated apoptosis in 5FU-resistant colorectal cancer cells. Oncol. Rep., 45: 680-692.
9. Chen, H.J., Y.L. Jiang, C.M. Lin, S.C. Tsai and S.F. Peng *et al*., 2013. Dual inhibition of EGFR and c-Met kinase activation by MJ-56 reduces metastasis of HT29 human colorectal cancer cells. Int. J. Oncol., 43: 141-150.
10. Mol, C.D., K.B. Lim, V. Sridhar, H. Zou and E.Y.T. Chien *et al*., 2003. Structure of a c-Kit product complex reveals the basis for kinase transactivation. J. Biol. Chem., 278: 31461-31464.
11. Du, Z. and C.M. Lovly, 2018. Mechanisms of receptor tyrosine kinase activation in cancer. Mol. Cancer, Vol. 17. 10.1186/s12943-018-0782-4.

12. Gajiwala, K.S., J.C. Wu, J. Christensen, G.D. Deshmukh and W. Diehl *et al*., 2009. KIT kinase mutants show unique mechanisms of drug resistance to imatinib and sunitinib in gastrointestinal stromal tumor patients. Proc. Nat. Acad. Sci. USA, 106: 1542-1547.
13. Imana, S.N., E.G. Ningsih and U.S.F. Tambunan, 2020. *In silico* identification of peptide as epidermal growth factor receptor tyrosine kinase inhibitors in lung cancer treatment. Pak. J. Biol. Sci., 23: 567-574.
14. Kansal, N., O. Silakari and M. Ravikumar, 2010. Three dimensional pharmacophore modelling for c-Kit receptor tyrosine kinase inhibitors. Eur. J. Med. Chem., 45: 393-404.
15. Yang, W. and L. Lai, 2017. Computational design of ligand-binding proteins. Curr. Opin. Struct. Biol., 45: 67-73.
16. Cui, W., A. Aouidate, S. Wang, Q. Yu, Y. Li and S. Yuan, 2020. Discovering anti-cancer drugs via computational methods. Front. Pharmacol., Vol. 11. 10.3389/fphar.2020.00733.
17. Joshi, T., T. Joshi, P. Sharma, S. Chandra and V. Pande, 2020. Molecular docking and molecular dynamics simulation approach to screen natural compounds for inhibition of *Xanthomonas oryzae* pv. oryzae by targeting peptide deformylase. J. Biomol. Struct. Dyn., 39: 823-840.
18. Lauro, G., M. Masullo, S. Piacente, R. Riccio and G. Bifulco, 2012. Inverse virtual screening allows the discovery of the biological activity of natural compounds. Bioorg. Medic. Chem., 20: 3596-3602.
19. Xu, X., M. Huang and X. Zou, 2018. Docking-based inverse virtual screening: methods, applications and challenges. Biophys. Rep., 4: 1-16.
20. Trott, O. and A.J. Olson, 2010. AutoDock Vina: Improving the speed and accuracy of docking with a new scoring function, efficient optimization and multithreading. J. Comput. Chem., 31: 455-461.
21. Sivashanmugam, M., K.N. Sulochana and V. Umashankar, 2018. Virtual screening of natural inhibitors targeting ornithine decarboxylase with pharmacophore scaffolding of DFMO and validation by molecular dynamics simulation studies. J. Biomol. Struct. Dyn., 37: 766-780.
22. Ahmed, M.Z., G. Muteeb, S. Khan, A.S. Alqahtani and P. Somvanshi *et al*., 2020. Identifying novel inhibitor of quorum sensing transcriptional regulator (SdiA) of *Klebsiella pneumoniae* through modelling, docking and molecular dynamics simulation. J. Biomol. Struct. Dyn., Vol. 39. 10.1080/07391102.2020.1767209.
23. Alonso, H., A.A. Bliznyuk and J.E. Gready, 2006. Combining docking and molecular dynamic simulations in drug design. Med. Res. Rev., 26: 531-568.
24. Peng, Y., Q. Chen, M. Gu, Y. Chen and M. Zhang *et al*., 2015. Human stromal cells in the peripheral zone of the prostate promote tumorigenesis of prostatic cancer stem cells through up-regulation of C-Kit expression. J. Cancer, 6: 776-785.
25. Stahtea, X.N., A.E. Roussidis, I. Kanakis, G.N. Tzanakakis and G. Chalkiadakis *et al*., 2007. Imatinib inhibits colorectal cancer cell growth and suppresses stromal-induced growth stimulation, MT1-MMP expression and pro-MMP2 activation. Int. J. Cancer, 121: 2808-2814.
26. Rishton, G.M., 2008. Molecular diversity in the context of leadlikeness: Compound properties that enable effective biochemical screening. Curr. Opin. Chem. Biol., 12: 340-351.
27. Meng, Y., Y.L. Lin and B. Roux, 2015. Computational study of the "DFG-Flip" conformational transition in c-Abl and c-Src tyrosine kinases. J. Phys. Chem. B, 119: 1443-1456.